Scattering of ultraviolet light by avian eggshells

Ladouce, Mathieu; Barakat, Tarek; Su, Bao Lian; Deparis, Olivier; Mouchet, Sébastien R.

Published in:
Faraday Discussions

DOI:
10.1039/d0fd00034e

Publication date:
2020

Document Version
Publisher's PDF, also known as Version of record

Faraday Discussions

Cite this: DOI: 10.1039/d0fd00034e

ROYAL SOCIETY OF CHEMISTRY

PAPER

View Article Online
View Journal

Scattering of ultraviolet light by avian eggshells†

Mathieu Ladouce,[a] Tarek Barakat,[b] Bao-Lian Su,[bcd] Olivier Deparis[a] and Sébastien R. Mouchet*[ae]

Received 9th March 2020, Accepted 11th May 2020
DOI: 10.1039/d0fd00034e

Eggshells are essential for the reproduction of birds since the optical properties of shells may have an impact on biological functions such as heating and UV protection, recognition by parents or camouflage. Whereas ultraviolet reflection by some bird eggshells has been recently described, its physical origin remains poorly understood. In this study, we identified a porous structure in eggshells. Using Mie scattering modelling, we found it was most likely responsible for reflectance peaks (intensities of *ca.* 20–50%) observed in the near-UV range. These peaks were observed by spectrophotometric measurements from eggshells of several breeds of hen, one breed of duck and one breed of quail. This optical response was interpreted in terms of the distinct visual perception of hens and humans: eggshells appearing achromatic for humans proved to be chromatic for hens. Fluorescence emission from these eggs was also characterised and attributed to the presence of protoporphyrin IX and biliverdin IXα in the shells. Electron microscopy observations revealed the presence of pores within the so-called calcified shell part (*i.e.*, at depths between *ca.* 20 μm and *ca.* 240 μm from the eggshell's outer surface). Mercury intrusion porosimetry allowed us to quantify the pore size distribution. Simulations of the UV response of this porous structure using Mie scattering theory as well as an effective approach accounting for multiple scattering indicate that these pores are responsible for the backscattering peaks observed in the UV range, in the case of beige hen eggshells. Due to the similarities between the pore size distributions observed for beige hen eggshells and other investigated poultry eggshells, we expect Mie backscattering to be the origin of the UV response of the eggshells of many other bird species.

[a]*Department of Physics, Namur Institute of Structured Matter (NISM), University of Namur, Rue de Bruxelles 61, 5000 Namur, Belgium. E-mail: sebastien.mouchet@unamur.be; Tel: +32 081 724722*

[b]*Laboratory of Inorganic Materials Chemistry (CMI), Namur Institute of Structured Matter (NISM), University of Namur, Rue de Bruxelles 61, 5000 Namur, Belgium*

[c]*State Key Laboratory of Advanced Technology for Materials Synthesis and Processing, Wuhan University of Technology, 122 Luoshi Road, Wuhan, Hubei 430070, China*

[d]*Department of Chemistry and Clare Hall College, University of Cambridge, Herschel Road, Cambridge CB3 9AL, UK*

[e]*School of Physics, University of Exeter, Stocker Road, Exeter EX4 4QL, UK. E-mail: s.mouchet@exeter.ac.uk*

† Electronic supplementary information (ESI) available. See DOI: 10.1039/d0fd00034e

Introduction

Ultraviolet radiation refers to a range of the electromagnetic spectrum between 10 nm and 400 nm, the longer wavelengths of which (close to the visible range, *ca.* 320–400 nm) can be perceived by many living organisms[1] such as insects and birds, but not mammals. As a consequence, many animals have evolved signalling functions in the near-UV range. For instance, some feathers,[2] hatchling skins[3] or butterfly wings[4–7] are known to strongly reflect UV, playing a role in mate choice or offspring care. Furthermore, exposure to UV (and specifically to UVB, *i.e.*, from 280 nm to 315 nm) has a detrimental effect on the DNA of living organisms. Therefore, depending on their habitat, it can be crucial for them to develop protection against this harmful radiation in order to avoid, for example, premature ageing of integuments, sunburn and cancer. The most common UV protection in animals is the use of pigments such as melanin. Other ways to protect against UV, such as nanometre-scale photonic structures, which also give rise to visual communication signals in the UV range, have evolved in various species (*i.e.*, birds,[2] butterflies,[4–9] spiders,[10] among many other examples[11–16]). Such natural photonic structures have diverse optical properties, including structural colours (*i.e.*, colours due to coherent scattering),[17,18] fluid-induced colour changes[19–22] or light polarisation effects.[23–25] However, the interaction between natural photonic structures and UV radiation has been investigated so far only in a few examples (*e.g.*, the bird *Ficedula hypoleuca*,[2] the jumping spider *Cosmophasis umbratica*,[10] as well as the butterflies *Eurema lisa*, *Chrysozephyrus* sp. and *Apatura* sp.[4–7]). Previously, it was shown that taking into account the UV range in the analysis of eggshell coloration revealed aspects of cuckoo–host egg matching that were unnoticeable using only human colour vision.[26] Despite such studies, the functional significance of strong UV scattering in the majority of other known UV-active biological materials is not understood.[27–29]

The physical properties of avian eggshells provide a wide range of biological functions favourable for bird reproduction, such as protection of the developing embryo from physical damage, controlled gas transfer, bacterial protection and calcium supply.[30–33] Avian eggshell is a structured and layered material;[30,34–36] the external layer (up to 20 μm deep) is the cuticle (which may contain pigments), the second layer is the "calcified shell" (which is mainly composed of calcite ($CaCO_3$)[30]), and the deepest layer is the outer membrane of the egg.

The various colourations of avian eggshells are usually reported to be due to three pigments: protoporphyrin IX (generally present in brown, light-brown, yellowish and reddish eggshells), biliverdin IXα (often associated with green, olive green and violet blue colourations) and biliverdin–zinc chelate (this pigment, however, is controversial and its detection may be due to the extraction method used in the reporting studies[37]), with occasional traces of mesobiliviolin, coproporphyrin III and other types of porphyrin.[38–41] Eggshell optical properties are crucial as they influence factors such as heating, UV protection, camouflage, recognition by parents and brood parasitism.[11,26,41–48] For instance, previous studies reported the influence of eggshell visual appearance, including the UV response and patterns, on mimicry and rejection mechanisms in the context of brood parasitism.[44,47,48]

Some preliminary observations of poultry species eggshells[27–29] revealed strong UV scattering, reaching up to 90% of the total reflectance at *ca.* 350 nm. This peak was only detected after the light-absorbing cuticle was dissolved in an acidic solution, namely ethylenediaminetetraacetic acid (EDTA). These studies also suggest that disordered spherical pores are involved in this UV scattering. However, the actual origin of the avian eggshell UV response has not yet been elucidated.

In this article, we characterised the optical properties (including UV reflection and fluorescence emission) of domestic hen (*Gallus gallus domesticus*), duck and quail eggshells (Fig. 1). We analysed the optical response in terms of the visual perception of humans and hens. We characterised the morphology of the porous structures presumed to be responsible for the UV scattering. Based on analytical predictions relying on Mie scattering theory and an effective approach accounting for multiple scattering, we predicted the optical behaviour in the UV range and compared it with experiments.

Materials and methods

Sample selection and preparation

We selected eggs from four breeds of hen (*G. gallus domesticus*) as well as one breed of duck and one breed of quail that were sourced from retail shops in the UK and Belgium (Fig. 1 and Table S1, ESI†). 21 samples were used for this study (beige hen eggs $n = 5$; brown hen eggs $n = 2$; white hen eggs $n = 6$; turquoise hen eggs $n = 2$; duck eggs $n = 2$; quail eggs $n = 4$). Eggshells were separated from their content by piercing small holes at both poles of the shells with a dissection needle. They were dissected and samples were taken from the equatorial areas, allowing the fragments to be as flat as possible. They were abundantly rinsed with water. Since quail eggshells display two distinct colour areas, namely brighter and darker regions, we performed independent experimental analyses of these areas.

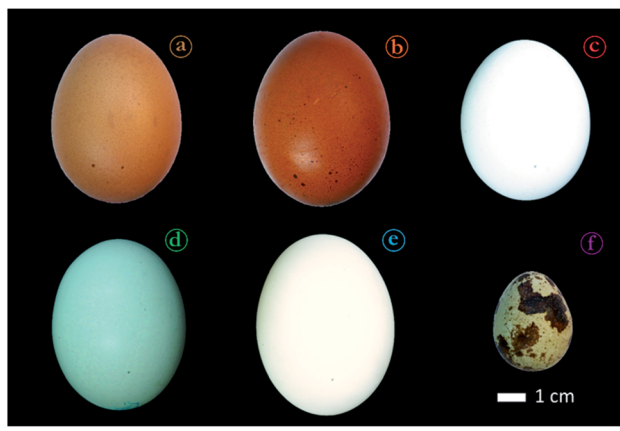

Fig. 1 Various visual appearances of avian eggshells. In this study, beige (a), brown (b), white (c) and turquoise (d) hen eggs, duck egg (e) and quail egg (f) were investigated.

Photography

Pictures were taken with a Pentax K10d digital reflex camera equipped with a Pentax D-FA macro lens (100 mm f2.8) under lighting by a halogen lamp. The white balance was adjusted with respect to a white diffusive surface.

Spectrophotometry

Total reflectance $R(\lambda)$, total transmittance $T(\lambda)$ and total absorption $A(\lambda)$ spectra were acquired with a PerkinElmer 750S UV/Vis/NIR spectrophotometer equipped with a 150 mm diameter integrating sphere and a deuterium–tungsten light source. Calibration was performed with a Labsphere SRS-99-020 white reference. Since the spectral region of interest lay within the UV range, we had to take into account possible fluorescence emission from the samples. Some eggshells were reported to emit by fluorescence decay.[38,39] If the samples were fluorescent, the detected intensity would be artificially increased in the UV range since the incidence wavelength was selected by a monochromator prior to the sample. Since the detector could not distinguish between photons at incident wavelength and fluorescence emission wavelength, the measured spectra could depart from the actual reflectance or transmittance spectra. In order to detect such problems, we also measured the specular reflection factors $r(\lambda) = (i(\lambda) - b(\lambda))/(w(\lambda) - b(\lambda))$ with an Avantes AvaSpec 2048 spectrophotometer, where $i(\lambda)$ and $w(\lambda)$ corresponded to the intensities reflected by the sample and by the Labsphere SRS-99-020 white reference, respectively, and $b(\lambda)$ was a noise correction. The reflection factor $r(\lambda)$ could be larger than 100% if the sample scattered light more directionally than the white reference. Samples were illuminated at normal incidence with an Ocean Optics DH-2000-BAL deuterium–tungsten light source through a bifurcated optical fibre. The integration time was selected by maximising the intensity of the signal in the limit of the detector saturation. Since the wavelength selection was performed after reflection on the sample in this case, photons emitted by fluorescence were detected at their emission wavelength. Comparing spectra measured with both instruments allowed us to qualitatively assess the influence of fluorescence emission on our measurements.

Avian and human quantum catches

A quantum catch Q_i is the relative amount of photons reflected by a surface and absorbed by a specific photoreceptor cell of a given species.[49–51] It can be calculated by:

$$Q_i = \frac{\int_{\lambda_1}^{\lambda_2} R(\lambda) S_i(\lambda) I(\lambda) d\lambda}{\int_{\lambda_1}^{\lambda_2} S_i(\lambda) I(\lambda) d\lambda},$$

where $R(\lambda)$ is the reflectance spectrum of the sample, $S_i(\lambda)$ is the spectral sensitivity of the photoreceptor cell,[52,53] $\lambda_1 = 300$ nm and $\lambda_2 = 700$ nm are the spectral range limits and $I(\lambda)$ was chosen to be the D_{65} illuminant defined by the CIE. Quantum catches for each photoreceptor of the human eye, *i.e.*, the Short, Medium and Long Wavelength Sensitive (SWS, MWS, LWS) photoreceptors,[52] were compared to those of *G. gallus domesticus*, *i.e.*, Very Short Wavelength Sensitive (VSWS), SWS, MWS and LWS photoreceptors.[53] In spite of the fact that

the perception of colours cannot be directly interpreted from quantum catches (since the brain transformation process of the optical signal into a perceived image is not accounted for), some analysis related to colour detection can be performed from these quantities.

Chemical treatment of the cuticle

The cuticles of some samples were thinned with 0.34 M (pH $\in$ [8.5, 9]) EDTA solution. The outer sides of the shells were placed facing the liquid, floating on the solution for various time durations (30 min, 60 min, 90 min and 120 min) so that the inner sides did not react with the EDTA solution. Since the cuticle slowly thinned upon contact with EDTA, an aqueous residue remained attached on the surface of the shell. At the end of the treatment, each sample was gently removed from the solution with soft paper and rinsed with distilled water.

Microspectrofluorometry and fluorescence quantum efficiency

Microspectrofluorometric measurements of eggshell surfaces were performed in order to determine their fluorescence emission intensity $I_{f,em}$ and to calculate the fluorescence quantum efficiencies ϕ_f. We used an Olympus BX61 optical microscope in fluorescence mode. In this specific configuration, UV light emitted by a Lumen Dynamics X-Cite Series 120PC Q source and filtered by a 360–380 $\pm$ 20 nm bandpass filter illuminated the sample. The backscattered and emitted photons were guided through the microscope into an Ocean Optics QE65 Pro spectrophotometer. The fluorescence quantum efficiency is the ratio of the number of photons emitted by fluorescence and the number of photons absorbed by the material:[51]

$$\phi_f = \frac{J_f}{J_0(I/I_0) - J},$$

where the different terms are:

$$J_f = \int_{420}^{800} I_{f,em}(\lambda)d\lambda;$$

$$J_0 = \int_{300}^{420} I_{S,0}(\lambda)d\lambda;$$

with $I_{S,0}(\lambda)$ the intensity that is backscattered by a Labsphere SRS-99-020 white reference when illuminated by the UV source and measured without the bandpass filter;

$$I_0 = \int_{760}^{800} I_{S,0}(\lambda)d\lambda;$$

$$I_0 = \int_{300}^{420} I_{S,sample}(\lambda)d\lambda;$$

with $I_{S,sample}(\lambda)$ the intensity that is backscattered by the sample when illuminated by the UV source and measured without the bandpass filter;

$$I = \int_{760}^{800} I_{S,sample}(\lambda)d\lambda.$$

The $J_0 - J$ factor is the difference between the number of photons reflected by the white reference and by the sample surface. This quantity must be integrated within the wavelength range corresponding to fluorescence excitation. Since the white reference has scattering properties that are different from those of the eggshells, the I/I_0 factor is introduced. The related integrals are in the range where the fluorescence emission is negligible compared to the reflection by the white reference or the sample surface. This correction factor is assumed to be independent of the wavelength. All the measured spectra, namely $I_{f,em}$, $I_{S,0}$ and $I_{S,sample}$, included noise corrections. Each spectrum was averaged on three acquisitions of 15 ms duration.

Spectrofluorometry

Fluorophores were extracted from eggshell samples by placing them in 0.34 M EDTA solutions for *ca.* 24 hours.[54] Fluorescence emission and excitation spectra of the extracts (100 μl) were measured using a PerkinElmer LS-45 spectrofluorometer. The excitation spectra were acquired between 250 nm and 320 nm with an emission wavelength λ_{em} corresponding to the maximum emission intensity. The emission spectra were measured between 300 nm and 800 nm with an excitation wavelength λ_{exc} corresponding to the maximum excitation intensity.

Electron microscopy and energy-dispersive X-ray spectroscopy

Scanning electron microscopy observations of the surface and the cross-sections of the samples were performed with a JEOL 7500 F in secondary electron detection mode. The 15 kV accelerating voltage of the incident beam gave rise to a theoretical lateral resolution of 1 nm. A thin layer (*ca.* 10 nm) of gold was deposited on the sample prior to any observation in order to avoid any charging effect. The chemical composition of beige hen eggshells was characterised by Energy-Dispersive X-ray spectroscopy (EDX) using this microscope. The analysis was performed across the shell cross-section and within the calcified shell. The analysis depth was assessed to $z_C = 2.93$ μm (carbon), $z_O = 4.18$ μm (oxygen) and $z_{Ca} = 3.87$ μm (calcium), using Castaing formula.[55]

Porosimetry

Samples of beige hen eggshells (size of about 2×2 mm^2) were analysed using a Micromeritics Autopore IV mercury intrusion porosimeter after treatment by 0.34 M EDTA solutions for *ca.* 24 hours. The outer membrane was removed mechanically.

Results and discussions

Optical characterisation

The colours of bird eggshells depend on the species as well as the breed (Fig. 1 and Table S1, ESI†). This diversity of visual appearances is observed in the measured total and specular reflectance spectra (Fig. 2). Despite the differences

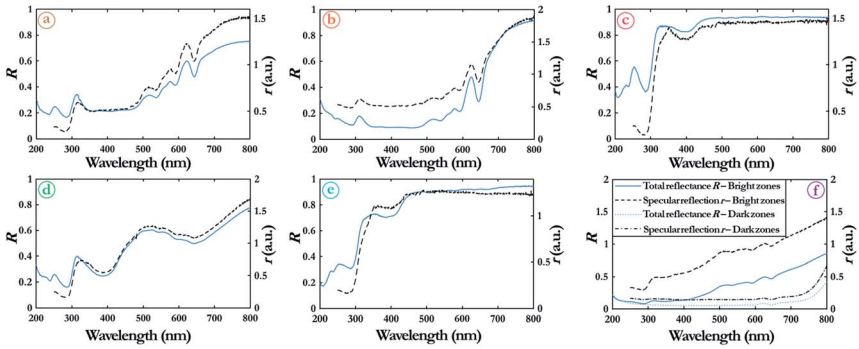

Fig. 2 Total reflectance (blue solid lines) and specular reflection coefficient (black dashed lines) spectra of beige (a), brown (b), white (c) and turquoise (d) hen eggshells, duck eggshell (e) and quail eggshell (f) exhibiting either a peak at both *ca.* 252 nm and 314 nm. The brighter and darker areas of quail eggshell were separately analysed. On average (n = 4), for beige hen eggshells, the first peak is observed at 250.8 ± 0.5 nm with 25.3 ± 4.1% total reflectance and the second peak is observed at 312.7 ± 2.7 nm with 32.3 ± 6.9% total reflectance. The standard error of the specular reflection coefficient was ±0.5% with a 0.63 nm spectral resolution.

among the species and breeds, a common feature appears for all eggshells in the UV range around 300 nm. In the cases of the beige, brown and turquoise hen eggshells, a 32.3 ± 6.9% reflectance peak is observed at 312.7 ± 2.7 nm. This peak spreads from 290 nm to 340 nm. In the cases of the white hen eggshells, the duck eggshells and the quail eggshells, the spectra exhibit a small peak in this range. In a previous study by Fecheyr-Lippens and coworkers,[27] similar behaviour was observed with hen and brushturkey eggs only after treatment of the eggshells by EDTA solution. In the eggshells selected for this study, similar UV responses were observed without this treatment. In addition, the reflectance spectra of the beige, white and turquoise hen eggshells, as well as the duck and quail eggshells, display another peak at 250.8 ± 0.5 nm that spreads from 235 nm to 275 nm.

Avian and human visual perception

One consequence of such optical behaviours in the UV range lies in the chromaticity of the eggshells' visual appearances, as revealed by the calculated quantum catches (Fig. S1, ESI†). Humans perceive the white hen eggshells and the duck eggshells as achromatic. However, the related visual appearances are detected as chromatic by *G. gallus domesticus*. Furthermore, eggshells that are chromatic for humans turn out to be also chromatic for hens. Finally, the calculated quantum catches indicate that the amounts of light that are absorbed by human and hen photoreceptors are similar. The colour of an eggshell that is perceived as intense by humans is also intense for hens.

Fluorescence emission and quantum efficiency

The eggshells of some species, including domestic hens, some ducks and quails, are known for being fluorescent.[38,39] In our investigation, we observed fluorescence emission from our samples under exposure to UV light (Fig. S2, ESI†).

Microspectrofluorometry measurements on the eggshell surfaces revealed the presence of an emission peak at *ca.* 475 nm for all the investigated eggshells (Fig. 3), while a second peak is observed in all spectra at *ca.* 665 nm. This common light emission behaviour indicates that the fluorophore compounds are similar for all samples. In addition, it suggests that either one or two kinds of fluorophore are embedded within the shells. If a single type of fluorophore exists in the shells, this fluorescent behaviour could be explained by two decay pathways, the influence of some photonic structures[56] or re-emission. Protoporphyrin IX and biliverdin IXα are very likely involved in the detected fluorescence emission. Both molecules, which are also usually responsible for eggshell pigmentary colours, were detected in the eggshells of hen, duck and quail, including (surprisingly) white eggs.[38,39] Protoporphyrin IX is well known for its red fluorescence and has been studied extensively for its biomedical relevance.[57,58] It emits light between 600 nm and 725 nm by fluorescence decay under incident light in the range of 400–420 nm.[57–59] To a much lesser extent, protoporphyrin IX is also reported to fluoresce between 300 nm and 320 nm when excited at 280–295 nm.[60] Biliverdin IXα is known to emit light between 400 nm and 550 nm under 375 nm wavelength excitation.[61]

This light emission by fluorescence decay has an influence on the total reflectance spectra measured with the PerkinElmer 750S UV/Vis/NIR spectrophotometer (Fig. 2) since the wavelength selection is performed in the incident light beam path. This influence had to be assessed since a strong fluorescence emission could be the origin of the peaks observed in the total reflectance spectra in the previous section. These spectra were compared (Fig. 2) with specular reflection factor spectra measured with an Avantes AvaSpec 2048 – for which the wavelength selection is performed in the detection beam path. Both kinds of spectra display similar behaviours. This allowed us to exclude the hypothesis according to which the peaks observed in the UV range are due to fluorescence emission.

Furthermore, the quantum efficiencies related to the selected eggshells (Fig. S3, ESI†) were assessed to be rather low for all the samples. The eggshells with the lightest colours – namely, white and turquoise hen eggshells, duck

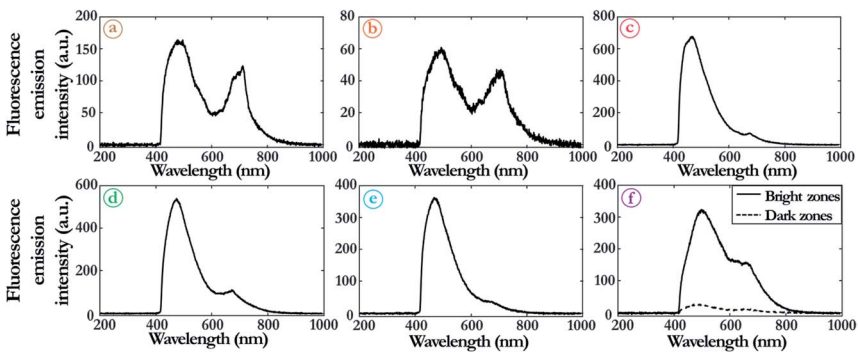

Fig. 3 Microspectrofluorometry measurements revealed fluorescence emission peaks at *ca.* 475 nm and 665 nm in all the investigated samples, namely beige (a), brown (b), white (c) and turquoise (d) hen eggshells, duck eggshell (e) and quail eggshell (f). The standard error of fluorescence emission intensity was ±0.1%.

eggshells and the bright area of quail eggshells – exhibit higher quantum efficiencies ranging from *ca.* 14% to *ca.* 26%. Darker shells, *i.e.*, the beige and brown hen eggshells, as well as the dark area of quail eggshells, display efficiencies lower than *ca.* 10%, most likely due to stronger light absorption in the eggshell materials.

Fluorescence excitation and emission spectra were measured for extracts from the investigated eggshells (Fig. 4). The excitation spectra of all extracts display a peak at *ca.* 280 nm. Due to the measurement set-up, we could not measure excitation spectra above 320 nm. Moreover, two peaks centred at *ca.* 345 nm and *ca.* 660 nm are observed in the emission spectra of all extracts. The former emission peak occurs at a wavelength shorter than that measured for the eggshells by microspectrofluorometry (*i.e.*, 475 nm). This difference in fluorescence emission peak wavelength could be explained by the difference in excitation light, by a change in the fluorophore chemical properties induced upon contact with EDTA, or by the influence of the photonic structure on emission properties.[56] The wavelength position of the second peak (at *ca.* 660 nm), however, is very close to that of the peak (at *ca.* 665 nm) in the microspectrofluorometry measurements. Fluorescence emission can be influenced when fluorophores are embedded in photonic structures.[24,56] In our case, the second fluorescence emission peak cannot be due to such light emission control as no photonic structure is present in the extracts. These excitation and emission properties also suggest the presence of either (1) only one kind of fluorophore within the eggshells, or (2) two different types of fluorophore with similar excitation properties in the investigated eggshells, so that the excitation of one type of fluorophore corresponds to the emission of the other.[62] The first scenario corresponds to a case where the measured fluorescence would only be due to protoporphyrin IX.[57–60] The second one is likelier and relates to the presence of both protoporphyrin IX and biliverdin IXα.[38,39]

Light absorption by the cuticle

A previous study[27] showed that a single backscattering peak appears in the UV range for selected egg species after treatment by EDTA solutions. Such

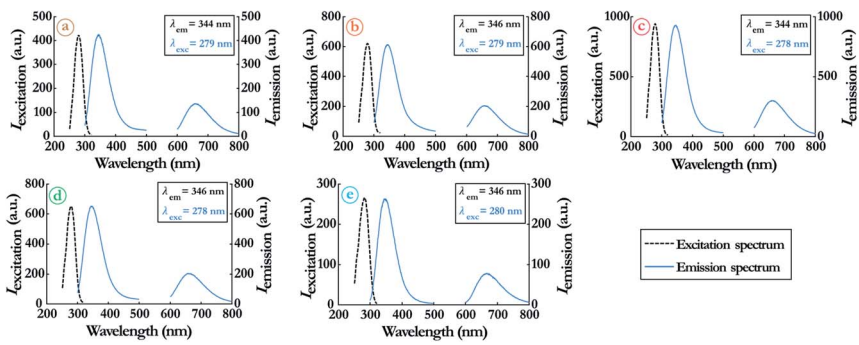

Fig. 4 The fluorescence excitation spectra measured from extracts of beige (a), brown (b), white (c) and turquoise (d) hen eggshells and duck eggshell (e) all exhibit a peak at *ca.* 280 nm. The corresponding emission spectra peak at *ca.* 345 nm and 660 nm, most likely due to the presence of protoporphyrin IX and biliverdin IXα. The standard error of the measured intensity was ±0.2% with 1 nm spectral resolution.

a treatment was described to thin the absorbing cuticle (which corresponds to a 20 μm-thick superficial layer). We measured the total reflectance and absorption spectra of beige hen eggshells (Fig. 5 and S4, ESI†) for different EDTA treatment durations (30 min, 60 min, 90 min and 120 min). This allowed us to assess whether the local minimum between the reflectance peaks measured at *ca.* 252 nm and *ca.* 314 nm is due to a light absorption band that would split a single backscattering peak at *ca.* 280 nm into the two peaks. SEM observations of the treated samples indicated that 60 min and 120 min treatment durations correspond to the dissolution of *ca.* 28 μm and *ca.* 41 μm, respectively (Fig. S5, ESI†). This implies that after 60 min, the 20 μm-thick absorbing cuticle is expected to be dissolved. The intensities of the reflectance peaks at *ca.* 252 nm and *ca.* 314 nm, as well as the intensity of the local minimum between them, increase with the duration of the chemical treatment. After 60 min, the peak at *ca.* 252 nm ($R = 97\%$) becomes more intense than that at *ca.* 314 nm ($R = 85\%$). We therefore conclude that the cuticle absorbs the incident UV light in a broadband manner, whereas the underlying calcified shell reflects it with a high scattering efficiency at two different wavelengths (*i.e., ca.* 252 nm and *ca.* 314 nm).

Pores in the calcified shells

The calcified shells of avian eggs are known to be porous.[27,29] In the cases of the beige, white and turquoise hen eggshells, SEM observations revealed the presence of pores over a thickness of *ca.* 220 μm, from *ca.* 20 μm below the outer surface of the shell (Fig. 6). Using image analysis software (ImageJ and the Analyze Particles subroutine[63]), the pore surface density was assessed to be $\sigma_{SEM} = 1.22\ \mu m^{-2}$ in the case of the beige hen eggshells. In addition, the mean radius was found to be $\bar{r}_{SEM} = 0.145 \pm 0.054$ μm, 0.121 ± 0.038 μm and 0.156 ± 0.046 μm for the beige, white and turquoise hen eggshells, respectively.

The pore size distribution was measured by mercury intrusion porosimetry in the case of beige hen eggshells (Fig. S6 and S7, ESI†). A fit using a Gaussian function led to a mean radius $\bar{r}_{Hg} = 204 \pm 4$ nm. This analysis revealed the presence of larger pores with a diameter of *ca.* 2 μm. They are most likely due

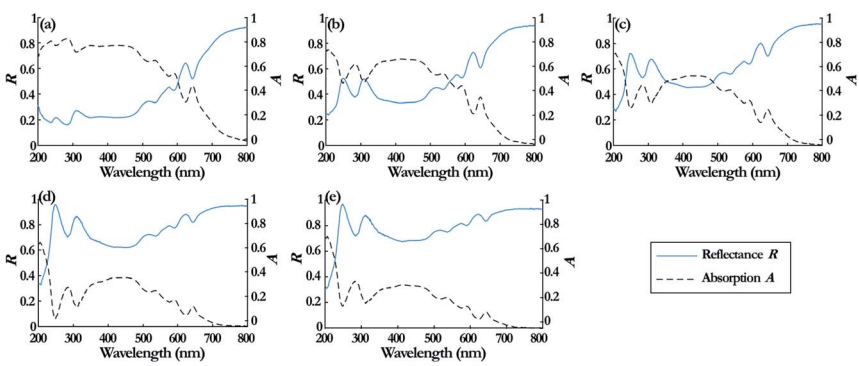

Fig. 5 The reflectance and absorption spectra measured for beige hen eggshell treated with 0.34 M EDTA for 0 min (control sample) (a), 30 min (b), 60 min (c), 90 min (d) and 120 min (e) indicate that the cuticle absorbs incident UV light, whereas the underlying calcified shell scatters UV light so that two peaks are observed at *ca.* 252 nm and 314 nm.

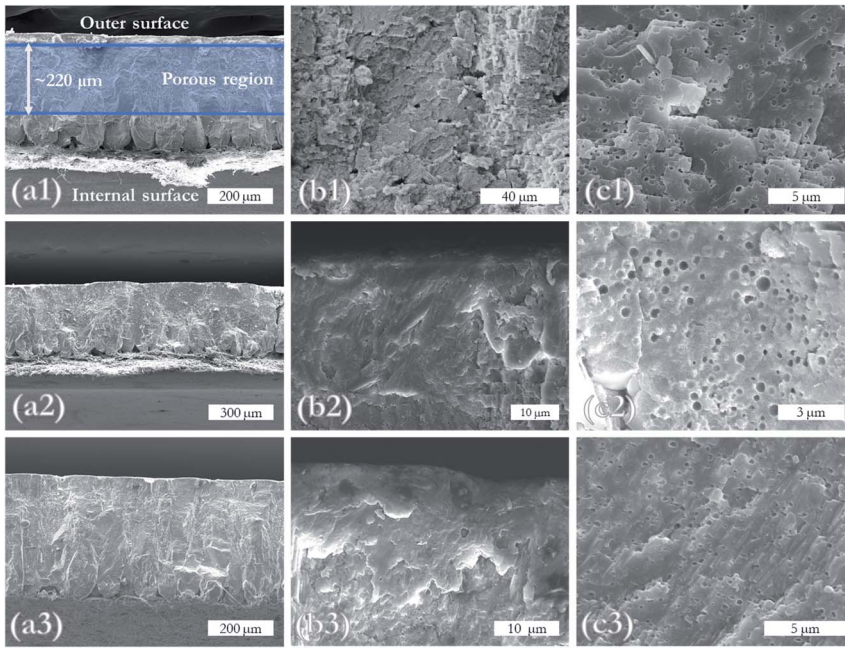

Fig. 6 SEM observations of the cross-section of beige (1), white (2) and turquoise (3) hen eggshells highlight the presence of pores in the calcified shells. Overview of the cross-section of eggshells (a); magnification of the calcified shell, revealing the pores (b); detailed overview of pores (c). The porous region of the eggshell spans a depth of *ca.* 20 μm to *ca.* 220 μm (a1, blue area) in the calcified shell.

to bigger channels in the calcified shell or to the surface roughness of the sample.

Chemical composition

Eggshells are usually thought to be mainly composed of amorphous calcite.[30] EDX analyses were performed on the cross-section of (a) the whole eggshell and (b) only the calcified shell, in the case of beige hen eggs (Table S2 and Fig. S9, ESI†). The EDX measurements indicate only small differences in concentrations of oxygen, calcium and carbon. The calcified shell is seemingly composed of pure calcite (O: 58.90%; Ca: 20.34%; C: 20.20%; other: 0.57%; Table S2, ESI†). Calcite is, however, not the only component of the rest of the eggshell, as the ratio of the number of carbon atoms and calcium atoms is *ca.* 1.5. This could be due to the presence of pigments, such as protoporphyrin IX ($C_{34}H_{34}N_4O_4$) or biliverdin IXα ($C_{33}H_{34}N_4O_6$).[38–40] Traces of other elements such as potassium, sodium, chlorine and magnesium were also detected, mainly in the analysis of the whole cross-section. They are probably due to biomolecules involved in the biological mechanisms of the morphogenesis of the cuticle or the external membrane, or they could be sample contaminants. No trace of zinc was detected in our analysis, excluding the presence of a zinc complex such as biliverdin–zinc chelate, which is a putative pigment occurring in eggshells.[37,54] The concentration profiles (Fig. S9, ESI†) indicate an increase in the carbon concentration and a decrease in the

calcium concentration at the interface between the calcified shell and the outer membrane. All profiles increase at a depth of *ca.* 65 μm from the outer surface and vary as a function of depth. These variations are likely due to surface roughness leading to shadowing effects and affecting the measurements.

Prediction of the UV response using Mie scattering theory

The porous structure observed in the investigated eggshells can be modelled by randomly distributed air spheres embedded in a calcite matrix. Such an optical model would be required to account for coherent effects resulting from each scatterer. As a preliminary approach, we considered an effective first Born approximation model of the structure where the multiple scattering properties are calculated by averages of single sphere scattering efficiencies obtained from Mie theory.[64] In this framework, the multiple scattering properties are characterised by the scattering mean free path l_t given by

$$l_t(\lambda) = \frac{1}{\rho\sigma(\lambda)},$$

where ρ is the density of the scatterers and $\sigma(\lambda)$ is the Mie scattering cross-section of a single scatterer. Mie theory predicts the scattering efficiencies of a single homogeneous sphere of radius a and refractive index $n_2(\lambda)$ surrounded by a medium with refractive index $n_1(\lambda)$.[65] Since the calcified shells are composed of amorphous calcite, we assumed $n_1(\lambda) = [n^{o}_{calcite}(\lambda) + n^{e}_{calcite}(\lambda)]/2$, where $n^{o}_{calcite}(\lambda)$ and $n^{e}_{calcite}(\lambda)$ are the ordinary and extraordinary refractive indices of crystalline calcite,[66] respectively, and $n_2 = n_{air} = 1$. We calculated the mean free path l_t using the equation above, assuming a sphere radius of $a = \bar{r}_{SEM} = 145$ nm and a sphere density of $\rho = 1.33 \times 10^{19}$ m^{-3}, corresponding to the measurements by mercury intrusion porosimetry.

The relationship between the scattering mean free path $l_t(\lambda)$ and the total transmittance $T_{tot}(\lambda)$ of light through the scattering medium can be expressed, in the first approximation, as:[67]

$$T_{tot}(\lambda) = \frac{l_t(\lambda) + z_e(\lambda)}{t + 2z_e(\lambda)},$$

where t is the thickness of the scattering medium and the extrapolation length is $z_e(\lambda) = 2l_t(\lambda)\alpha(\lambda)/3$ with a correction factor $\alpha(\lambda)$ for internal reflections. Using this equation allows us to assess the mean free path $l_t(\lambda)$ in calcified shells based on measurements of the total transmittance spectra $T_{tot}(\lambda)$ of beige hen eggshell (Fig. 5). For this purpose, we used the samples that were treated in EDTA solution for 120 min (Fig. 5e). Assuming a thickness of the calcified shell equal to $t = 220$ μm and a thickness of the eggshell equal to $d = 400$ μm (Fig. 6), we added a Beer–Lambert correction to the measured total transmittance $T_{tot}(\lambda)$ corresponding to the extinction in the non-scattering layers:

$$T^{corr}_{tot}(\lambda) = T_{tot}(\lambda)e^{(d-t)\kappa_{ext}(\lambda)},$$

where $\kappa_{ext}(\lambda)$ is the extinction coefficient calculated from absorption measurements (Fig. 5e). From the comparison between the scattering mean free path calculated from the Mie scattering cross-section of a single scatterer and the scattering mean free path assessed by the measured total transmittance (Fig. S10,

ESI†), we are confident of the reliability of an effective model accounting for the optical properties of light scatterers in the range of interest.

Scattering efficiencies

In the framework of an effective model of the porous structure observed in the calcified shells, predictions of the optical response can be performed in the first Born approximation from Mie theory. The scattering efficiency $Q_{\mathrm{Sca}}(\lambda,a,n)$ (with $n = n_2/n_1$) of a single spherical scatter,[65] which we calculated as a function of the sphere radius and the wavelength, displays two resonance modes (Fig. 7a). In order to take into account the size distribution of the pores, we calculated the weighted average of the scattering efficiency $S_{\mathrm{Sca}}(\lambda)$ (Fig. 7c):

$$S_{\mathrm{Sca}}(\lambda) = \frac{\int Q_{\mathrm{Sca}}(\lambda, a, n)\gamma(a)\mathrm{d}a}{\int \gamma(a)\mathrm{d}a},$$

where $\gamma(a)$ is a Gaussian distribution function that fits to the experimental pore radius distribution measured for beige hen eggshells (Fig. S6b, ESI†). The resulting weighted average spectrum exhibits no specific scattering peaks around 252 nm or 314 nm (Fig. 7c). However, the backscattering efficiency $Q_{\mathrm{b}}(\lambda,a,n)$[65] displays multiple resonance modes (Fig. 7b) and the resulting weighted average spectrum of the backscattering efficiency $S_{\mathrm{b}}(\lambda)$ exhibits a peak and a local maximum close to the wavelengths of the reflectance peak maxima observed in the measured total reflectance spectra (Fig. 7d). This result indicates that a Gaussian distribution of air spheres embedded in an amorphous calcite matrix can backscatter UV light with a high efficiency at wavelengths close to the total reflectance peaks measured for beige hen eggshells. Our analysis showed that the

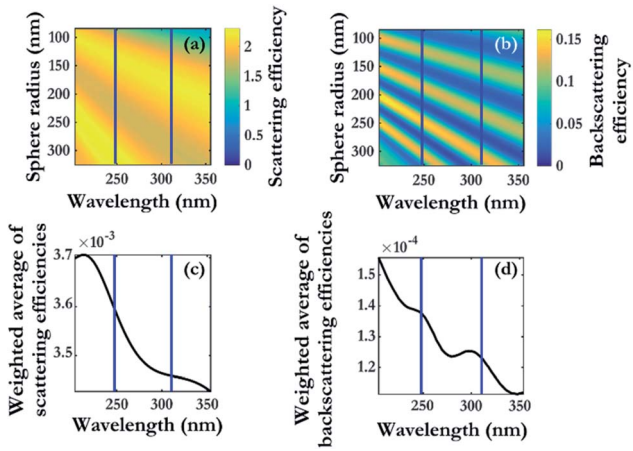

Fig. 7 The scattering (a) and backscattering (b) efficiency maps of air spheres embedded in amorphous calcite exhibit several Mie resonance modes that depend on the incident light wavelength and the sphere radius. The sphere radius range is centred on the mean pore radius of the distribution measured by porosimetry. The weighted averages of scattering (c) and backscattering (d) efficiencies allow us to account phenomenologically for multiple scattering. Vertical blue lines represent the wavelengths of reflectance peaks measured on beige hen eggshells (*i.e.*, 252 nm and 314 nm).

Table 1 The comparison between the ratios r_R, r_b and r_{Sca} indicates that the response measured in the UV range corresponds to backscattering. λ_{P1} and λ_{P2} are (1) for r_R, the wavelengths of the total reflectance peaks in the spectrum of the beige hen eggshell treated by EDTA solution for 120 min (*i.e.*, $\lambda_{P1} = 248$ nm and $\lambda_{P2} = 311$ nm); or (2) for r_b and r_{Sca}, the wavelengths of the peak and the local maximum of the weighted average of (back) scattering efficiencies (*i.e.*, $\lambda_{P1} = 245$ nm and $\lambda_{P2} = 303$ nm)

	λ_{P1}	λ_{P2}	Ratios
$R(\lambda)$	97.1%	88.4%	$r_R = 1.10$
$S_b(\lambda)$	1.38×10^{-4}	1.25×10^{-4}	$r_b = 1.10$
$S_{Sca}(\lambda)$	3.62×10^{-4}	3.47×10^{-4}	$r_{Sca} = 1.04$

pore size distribution is the most sensitive parameter in the model. Since similar pore size distributions were observed in the other investigated eggshells (Fig. 6), we can anticipate similar results for the other cases. As we observed similar optical behaviours in the UV range for the other eggshells (Fig. 2), we expect Mie backscattering to be also the origin of the UV response of the eggshells of other poultry (and more generally bird) species.

Moreover, we can reasonably assume a linear scaling between the weighted average of the backscattering efficiency (predicted) and the total reflectance (measured). If $R(\lambda)$ and $S(\lambda)$ values cannot be directly compared, the following ratios can be compared thanks to linear scaling: $r_R = R(\lambda_{P1})/R(\lambda_{P2})$ (where $R(\lambda)$ is the measured total reflectance of the beige hen eggshell treated by EDTA solution for 120 min (Fig. 5e), and λ_{P1} and λ_{P2} are the wavelengths of the optical response peaks); $r_b = S_b(\lambda_{P1})/S_b(\lambda_{P2})$; and $r_{Sca} = S_{Sca}(\lambda_{P1})/S_{Sca}(\lambda_{P2})$. All three ratios are within the range 1.04–1.10 (Table 1); r_b is closer to r_R than r_{Sca}, which is expected due to the definitions of these physical quantities, in terms of light propagation directions. The agreement between r_b and r_R is excellent and is a further indication that the observed response in the UV range is due to backscattering.

Conclusions

Two reflectance peaks were observed in the near-UV range by spectrophotometric measurements of eggshells of different breeds of hen, one breed of duck and one breed of quail without any preliminary dissolution of their cuticles. This strong UV reflection could have an influence on biological functions such as UV protection, camouflage or recognition by parents, since the UV response of the investigated eggshells were shown to be most likely detected by hen eyes. Eggshells perceived as achromatic by humans proved to be chromatic for hens. Progressively thinning the cuticle of beige hen eggshells allowed us to show that the so-called calcified shell is an efficient UV scattering structure, whereas the cuticle partly absorbs UV radiation. These eggs also exhibit fluorescence emission under UV incident light, most likely due to the presence of protoporphyrin IX and biliverdin IXα in the shell. SEM observations of cross-sections of the investigated eggshells revealed a microporous structure embedded in the calcified shell. The size distribution of these pores was quantified by mercury intrusion porosimetry. Finally, predictions of the optical properties of the porous structure of beige hen eggshells were performed using an effective first Born approximation modelling

approach. Multiple scattering was approximated by averaging the Mie backscattering response of single air spheres in amorphous calcite over the scatterer size distribution using a Gaussian weight function. The good match between these predictions and the measurements strongly indicates that the pores observed in avian eggshells are the origin of the optical response measured in the UV range. Due to the similarities between the pore size distributions observed for beige hen eggshells and the other investigated eggshells, we expect Mie backscattering to be the origin of the UV response of the eggshells of other bird species.

Conflicts of interest

There are no conflicts to declare.

Acknowledgements

The authors thank C. Charlier (Electron Microscopy Service, UNamur) and A. Fattaccioli (Department of Biology, UNamur) for technical support during the electron microscopy observations and the spectrofluorometry measurements of the extracts, respectively. D. B. Colridge (School of Physics, University of Exeter) and M. D. Shawkey (Department of Biology, Ghent University) are also thanked for reading the manuscript and for fruitful discussions, respectively. S. R. M. was supported by the Belgian National Fund for Scientific Research (FRS-FNRS) as a Postdoctoral Researcher (91400/1.B.309.18F). This research was also supported by FRS-FNRS through the Researchers' Credit CC 1.5075.11F. This research used the resources of the Technological Platform High Performance Computing (PTCI) (http://www.ptci.unamur.be) located at UNamur and the resources of the Electron Microscopy Service (SME) of UNamur (http://www.unamur.be/en/sevmel). PTCI is supported by FNRS-FRFC, the Walloon Region and UNamur (Conventions No. 2.5020.11, GEQ U.G006.15, 1610468 and RW/GEQ2016). PTCI and SME are members of the "Consortium des Équipements de Calcul Intensif (CÉCI)" (http://www.ceci-hpc.be) and the Technological Platform Morphology-Imaging (MORPH-IM) of UNamur, respectively.

Notes and references

1 M. B. Toomey, O. Lind, R. Frederiksen, R. W. Curley Jr, K. M. Riedl, D. Wilby, S. J. Schwartz, C. C. Witt, E. H. Harrison, N. W. Roberts, M. Vorobyev, K. J. McGraw, M. C. Cornwall, A. Kelber and J. C. Corbo, *eLife*, 2016, **5**, e15675.
2 H. Siitari and E. Huhta, *Behav. Ecol.*, 2002, **13**, 737–741.
3 V. Jourdie, B. Moureau, A. T. D. Bennett and P. Heeb, *Nature*, 2004, **431**, 262.
4 H. Ghiradella, D. Aneshansley, T. Eisner, R. E. Silberglied and H. E. Hinton, *Science*, 1972, **178**, 1214–1217.
5 M. Imafuku, Y. Hirose and T. Takeuchi, *Zool. Sci.*, 2002, **19**, 175–183.
6 D. Pantelić, S. Ćurčić, S. Savić-Šević, A. Korać, A. Kovačević, B. Ćurčić and B. Bokić, *Opt. Express*, 2011, **19**, 5817–5826.
7 F. Schenk and D. G. Stavenga, *Faraday Discuss.*, 2020, DOI: 10.1039/D0FD00036A.
8 H. Ghiradella, *Appl. Opt.*, 1991, **30**, 3492–3500.
9 P. Pirih, B. D. Wilts and D. G. Stavenga, *J. Comp. Physiol., A*, 2011, **197**, 987–997.

10 M. F. Land, J. Horwood, M. L. M. Lim and D. Li, *Proc. R. Soc. London, Ser. B*, 2007, **274**, 1583–1589.
11 J. M. Avilés, J. J. Soler and T. Pérez-Contreras, *Proc. R. Soc. London, Ser. B*, 2006, **273**, 2821–2829.
12 G. T. van de Kerkhof, L. Schertel, R. Poon, G. Jacucci, B. J. Glover and S. Vignolini, *Faraday Discuss.*, 2020, DOI: 10.1039/D0FD00024H.
13 R. B. Primack, *Arnoldia*, 1982, **42**, 139–146.
14 J.-P. Vigneron, M. Rassart, Z. Vértesy, K. Kertész, M. Sarrazin, L. P. Biró, D. Ertz and V. Lousse, *Phys. Rev. E*, 2005, **71**, 011906.
15 M. E. Inchaussandague, D. C. Skigin, A. Tolivia, I. Fuertes Vila and V. Conforti, *Proc. SPIE*, 2014, **9055**, 905514.
16 A. V. Zabuga, M. I. Arrigo, J. Teyssier, S. R. Mouchet, K. Nishikawa, M. Matsui, M. Vences and M. C. Milinkovitch, *Soft Matter*, 2020, **16**, 1714–1721.
17 S. Kinoshita, *Structural Colors in the Realm of Nature*, World Scientific, 2008.
18 S. R. Mouchet and P. Vukusic, *Adv. Insect Physiol.*, 2018, **54**, 1–53.
19 J.-P. Vigneron, J. M. Pasteels, D. M. Windsor, Z. Vértesy, M. Rassart, T. Seldrum, J. Dumont, O. Deparis, V. Lousse, L. P. Biró, D. Ertz and V. Welch, *Phys. Rev. E*, 2007, **76**, 031907.
20 S. R. Mouchet, E. Van Hooijdonk, V. L. Welch, P. Louette, J.-F. Colomer, B.-L. Su and O. Deparis, *Sci. Rep.*, 2016, **6**, 1–10.
21 R. A. Potyrailo, H. Ghiradella, A. Vertiatchikh, K. Dovidenko, J. R. Cournoyer and E. Olson, *Nat. Photonics*, 2007, **1**, 123–128.
22 S. R. Mouchet, T. Tabarrant, S. Lucas, B.-L. Su, P. Vukusic and O. Deparis, *Opt. Express*, 2016, **24**, 12267–12280.
23 S. A. Jewell, P. Vukusic and N. W. Roberts, *New J. Phys.*, 2007, **9**, 99.
24 S. R. Mouchet, C. Verstraete, D. Mara, S. Van Cleuvenbergen, E. D. Finlayson, R. Van Deun, O. Deparis, T. Verbiest, B. Maes, P. Vukusic and B. Kolaric, *Interface Focus*, 2019, **9**, 20180052.
25 B. Winter, B. Butz, C. Dieker, G. E. Schröder-Turk, K. Mecke and E. Spiecker, *Proc. Natl. Acad. Sci. U. S. A.*, 2015, **112**, 12911–12916.
26 M. I. Cherry and T. D. Bennett, *Proc. R. Soc. London, Ser. B*, 2001, **268**, 565–571.
27 D. C. Fecheyr-Lippens, B. Igic, L. D'Alba, D. Hanley, A. Verdes, M. Holford, G. I. N. Waterhouse, T. Grim, M. E. Hauber and M. D. Shawkey, *Biol. Open*, 2015, **4**, 753–759.
28 B. Igic, D. Fecheyr-Lippens, M. Xiao, A. Chan, D. Hanley, P. R. L. Brennan, T. Grim, G. I. N. Waterhouse, M. E. Hauber and M. D. Shawkey, *J. R. Soc., Interface*, 2015, **12**, 20141210.
29 L. D'Alba, R. Torres, G. I. N. Waterhouse, C. Eliason, M. E. Hauber and M. D. Shawkey, *Physiol. Biochem. Zool.*, 2017, **90**, 588–599.
30 C. Tyler, in *International Review of General and Experimental Zoology*, ed. W. J. L. Felts and R. J. Harrison, Elsevier, 1969, vol. 4, pp. 81–130.
31 M. Ketta and E. Tůmová, *Czech J. Anim. Sci.*, 2016, **61**, 299–309.
32 M. C. Stoddard, E. H. Yong, D. Akkaynak, C. Sheard, J. A. Tobias and L. Mahadevan, *Science*, 2017, **356**, 1249–1254.
33 L. D'Alba, D. N. Jones, H. T. Badawy, C. M. Eliason and M. D. Shawkey, *J. Exp. Biol.*, 2014, **217**, 1116–1121.
34 S. G. Tullett, *Comp. Biochem. Physiol., Part A*, 1984, **78**, 5–13.
35 M. Panheuleux, M. Bain, M. S. Fernandez, I. Morales, J. Gautron, J. L. Arias, S. E. Solomon, M. Hincke and Y. Nys, *Br. Poult. Sci.*, 1999, **40**, 240–252.

36 P. D. G. Richards and D. C. Deeming, *Br. Poult. Sci.*, 2001, **42**, 338–343.
37 T. Baird, S. E. Solomon and D. R. Tedstone, *Br. Poult. Sci.*, 1975, **16**, 201–208.
38 G. Y. Keneddy and H. G. Vevers, *Comp. Biochem. Physiol., Part B*, 1973, **44**, 11–25.
39 G. Y. Kennedy and H. G. Vevers, *Comp. Biochem. Physiol., Part B*, 1976, **55**, 117–123.
40 N. H. C. Sparks, *Avian Biol. Res.*, 2011, **4**, 162–167.
41 M. E. Hauber, A. L. Bond, A.-L. Kouwenberg, G. J. Robertson, E. S. Hansen, M. Holford, M. Dainson, A. Luro and J. Dale, *J. R. Soc., Interface*, 2019, **16**, 20190115.
42 J. Moreno and J. L. Osorno, *Ecol. Lett.*, 2003, **6**, 803–806.
43 R. M. Kilner, *Biol. Rev.*, 2006, **81**, 383–406.
44 M. C. Stoddard and M. Stevens, *Evolution*, 2011, **65**, 2004–2013.
45 P. Cassey, G. H. Thomas, S. J. Portugal, G. Maurer, M. E. Hauber, T. Grim, P. G. Lovell and I. Mikšík, *Biol. J. Linn. Soc.*, 2012, **106**, 657–672.
46 G. Maurer, S. J. Portugal, M. E. Hauber, I. Mikšík, D. G. D. Russell and P. Cassey, *Funct. Ecol.*, 2015, **29**, 209–218.
47 P. Cassey, M. Honza, T. Grim and M. E. Hauber, *Biol. Lett.*, 2008, **4**, 515–517.
48 M. C. Stoddard and M. Stevens, *Proc. R. Soc. London, Ser. B*, 2010, **277**, 1387–1393.
49 M. Vorobyev and D. Osorio, *Proc. R. Soc. London, Ser. B*, 1998, **265**, 351–358.
50 M. Vorobyev, J. Marshall, D. Osorio, N. Hempel de Ibarra and R. Menzel, *Color Res. Appl.*, 2001, **26**, S214–S217.
51 A. Iriel and M. G. Lagorio, *Naturwissenschaften*, 2010, **97**, 915–924.
52 A. Stockman and L. T. Sharpe, *Vision Res.*, 2000, **40**, 1711–1737.
53 D. Wilby, M. B. Toomey, P. Olsson, R. Frederiksen, M. C. Cornwall, R. Oulton, A. Kelber, J. C. Corbo and N. W. Roberts, *J. R. Soc., Interface*, 2015, **12**, 20150591.
54 A. Gorchein, C. K. Lim and P. Cassey, *Biomed. Chromatogr.*, 2009, **23**, 602–606.
55 J. Faerber, *Microscopie électronique à balayage - Microanalyse X par sonde électronique*, Institut de Physique et Chimie des Matériaux de Strasbourg, 2004.
56 S. R. Mouchet, M. Lobet, B. Kolaric, A. M. Kaczmarek, R. Van Deun, P. Vukusic, O. Deparis and E. Van Hooijdonk, *Proc. R. Soc. London, Ser. B*, 2016, **283**, 20162334.
57 K. R. Rollakanti, S. C. Kanick, S. C. Davis, B. W. Pogue and E. V. Maytin, *Photonics Lasers Med.*, 2013, **2**, 287–303.
58 R. M. Valentine, S. H. Ibbotson, K. Wood, C. T. A. Brown and H. Moseley, *Photochem. Photobiol. Sci.*, 2013, **12**, 203–213.
59 F. R. de Oliveira Silva, M. H. Bellini, V. R. Tristão, N. Schor, N. D. Vieira and L. C. Courrol, *J. Fluoresc.*, 2010, **20**, 1159–1165.
60 L. Sułkowski, B. Pawełczak, M. Chudzik and M. Maciążek-Jurczyk, *Molecules*, 2016, **21**, 1519.
61 S. Ghosh, C.-L. Yu, D. J. Ferraro, S. Sudha, S. K. Pal, W. F. Schaefer, D. T. Gibson and S. Ramaswamy, *Proc. Natl. Acad. Sci. U. S. A.*, 2016, **113**, 11513–11518.
62 S. R. Mouchet, A. M. Kaczmarek, D. Mara, R. V. Deun and P. Vukusic, *Proc. SPIE*, 2019, **10965**, 109650C.
63 C. A. Schneider, W. S. Rasband and K. W. Eliceiri, *Nat. Methods*, 2012, **9**, 671–675.

64 E. Akkermans and G. Montambaux, *Mesoscopic Physics of Electrons and Photons*, Cambridge University Press, 2007.
65 C. F. Bohren and D. R. Huffman, *Absorption and Scattering of Light by Small Particles*, Wiley-VCH Verlag GmbH, 2007.
66 G. Ghosh, *Opt. Commun.*, 1999, **163**, 95–102.
67 M. Burresi, L. Cortese, L. Pattelli, M. Kolle, P. Vukusic, D. S. Wiersma, U. Steiner and S. Vignolini, *Sci. Rep.*, 2014, **4**, 1–8.

